

# Quantum spin Hall effect in rutile-based oxide multilayers

J. L. Lado,<sup>1</sup> Daniel Guterding,<sup>2</sup> Paolo Barone,<sup>3,4</sup> Roser Valentí,<sup>2</sup> and V. Pardo<sup>5,6</sup>

<sup>1</sup>*QuantaLab, International Iberian Nanotechnology Laboratory, Braga, Portugal\**

<sup>2</sup>*Institut für Theoretische Physik, Goethe-Universität Frankfurt,  
Max-von-Laue-Straße 1, 60438 Frankfurt am Main, Germany†*

<sup>3</sup>*Consiglio Nazionale delle Ricerche (CNR-SPIN), 67100 L'Aquila, Italy*

<sup>4</sup>*Graphene Labs, Istituto Italiano di Tecnologia, via Morego 30, 16163 Genova, Italy*

<sup>5</sup>*Departamento de Física Aplicada, Universidade de Santiago de Compostela,  
E-15782 Campus Sur s/n, Santiago de Compostela, Spain*

<sup>6</sup>*Instituto de Investigacións Tecnolóxicas, Universidade de Santiago de Compostela,  
E-15782 Campus Sur s/n, Santiago de Compostela, Spain*

Dirac points in two-dimensional electronic structures are a source for topological electronic states due to the  $\pm\pi$  Berry phase that they sustain. Here we show that two rutile multilayers (namely  $(\text{WO}_2)_2/(\text{ZrO}_2)_n$  and  $(\text{PtO}_2)_2/(\text{ZrO}_2)_n$ , where an active bilayer is sandwiched by a thick enough ( $n=6$  is sufficient) band insulating substrate, show semi-metallic Dirac dispersions with a total of four Dirac cones along the  $\Gamma - M$  direction. These become gapped upon the introduction of spin-orbit coupling, giving rise to an insulating ground state comprising four edge states. We discuss the origin of the lack of topological protection in terms of the valley spin-Chern numbers and the multiplicity of Dirac points. We show with a model Hamiltonian that mirror-symmetry breaking would be capable of creating a quantum phase transition to a strong topological insulator, with a single Kramers pair per edge.

## I. INTRODUCTION

Topological states of matter<sup>1,2</sup> have been the source of tremendous excitement and have fostered a rich variety of new (and old) ideas in condensed matter physics. Quantum Hall effect, quantum spin Hall states,<sup>3</sup> topological crystals and topological crystalline insulators are some examples in which the topology of the single-electron Hamiltonian translates into robust electronic transport and surface states, resilient to the typical perturbations that real samples will have, such as defects and impurities. The different types of quantum Hall effects have provided us with a way to easily measure the quality of samples and even the charge of the electron, whereas quantum spin Hall states realize chiral wires,<sup>3</sup> where momentum and spin are coupled together. Furthermore, their superconducting analogues, topological superconductors<sup>4</sup> are known to give rise to Majorana bound states.<sup>5</sup> Such many-body states can show non-abelian braiding properties, making them suitable to become building blocks for topological quantum computing. Moreover, the nature of some of these topological states in superconductors still needs to be understood.<sup>6</sup> A common way to design topological superconductors is precisely based on a quantum spin Hall state proximized to a conventional superconductor,<sup>4</sup> turning quantum spin Hall states into a key ingredient not only in spintronics,<sup>7</sup> but also in topological quantum computing.

Two main mechanisms need to be understood in order to design quantum spin Hall states. The first one corresponds to band inversion, which relies on spin-orbit coupling (SOC) altering the order of the  $s-p$  orbital characters in a band structure, whose best known realization are HgTe/CdTe quantum wells.<sup>8</sup> The modification can occur at the  $\Gamma$  point, so that SOC basically changes the

parity of the highest occupied band. The second mechanism is the opening of a protected Dirac point by SOC.<sup>3</sup> Dirac points host protected  $\pm\pi$  Berry phases that become  $\pm 1/2$  Chern numbers upon a gap opening, so that in the presence of time-reversal symmetry a total spin-Chern number gives rise to the quantum spin Hall state, whereas with broken time reversal symmetry a quantum anomalous Hall state is realized.

The theoretical quest for new topological insulators has involved semiconductors<sup>9,10</sup>, transition metal oxides,<sup>11</sup> metal organic frameworks<sup>12,13</sup> or optical lattices.<sup>14</sup> Among them, oxides offer a rich set of possibilities due to the variety of materials that can be synthesized in a chemically stable form, together with the ease of fabrication in low-dimensional forms such as thin films or multilayers. Predictions of both, quantum spin Hall and quantum anomalous Hall effect have appeared in various oxides based on perovskites,<sup>15–17</sup> pyrochlores,<sup>11,18</sup> rutiles,<sup>19</sup> corundum<sup>20</sup> or doped Kagome structure.<sup>21</sup> Many of the proposals rely on an underlying hexagonal lattice, where Dirac points are prone to appear at the  $K, K'$  corners of the Brillouin zone. Rutiles, however, develop (semi) Dirac points, but due to their tetragonal unit cell, the Dirac points show up at a certain  $k$ -point in the  $\Gamma - X$  direction.<sup>22</sup> Opening a gap at these points with a time-reversal symmetry breaking has been shown to give rise to a quantum anomalous Hall state<sup>19</sup> with a very small gap of about 1 meV. Whether a quantum spin Hall state in a rutile-based structure can be engineered or not in such a way is still an open issue.

In this manuscript we address whether a rutile material with time-reversal symmetry is able to develop a quantum spin Hall state by opening a gap at the Dirac points of its band structure by the SOC effect. For that sake, we have designed two different rutile multi-

layers that show Dirac points in their band structure, i.e.  $(\text{WO}_2)_2/(\text{ZrO}_2)_4$  and  $(\text{PtO}_2)_2/(\text{ZrO}_2)_4$ . Both heterostructures become gapped upon introduction of SOC. We show by means of their topological invariants and the calculation of their edge states, that both systems realize a 2D crystalline topological insulating state, characterized by four in-gap surface states. We discuss the origin of this insulating state in terms of the spin valley Chern numbers, whose multiplicity is determined by the symmetry of the unit cell. We propose a model Hamiltonian to describe the system and we show that breaking an in-plane mirror symmetry can drive a transition towards a strong topological insulator by compensating two of the Dirac points and leaving just two of them with uncompensated spin valley Chern numbers.

## II. GAPPED DIRAC POINTS IN NON-MAGNETIC RUTILES

The multilayers proposed (see Fig. 1a) are based on the rutile structure and grow along the (001) direction with the  $a, b$  lattice parameters fixed to those of the band insulating substrate and the  $c$ -axis and internal atomic positions fully relaxed. We use as insulating substrate rutile  $\text{ZrO}_2$  whose bulk lattice parameters were calculated *ab initio* (see Methods section) yielding  $a = 4.93$  Å, which was the used value. The only requisite that the substrate should have is to provide a substantial gap where the  $d$  electrons of the active bilayer are allowed to form the Fermi surface without mixing with the states of the substrate. We have tried other substrates, e.g.  $\text{TiO}_2$  would be a good candidate in terms of the size of its band gap. However, the band bending it introduces will be so large that it would destroy the Dirac points.  $\text{TiO}_2$  with a slightly enlarged  $a$  parameter would be fine for our purposes, or even a very thin layer of  $\text{ZrO}_2$  on top of  $\text{TiO}_2$  would also do.  $\text{WO}_2$  on top of  $\text{ZrO}_2$  would be almost unstrained ( $a = 4.86$  Å), but  $\text{PtO}_2$  would undergo substantial strain since our calculations yields  $a = 4.59$  Å. We have also tried other insulating substrates, such as  $\text{SnO}_2$  and  $\text{PbO}_2$ , whose lattice matching will be better than  $\text{ZrO}_2$ , but their very narrow gap destroys the Dirac points by mixing substantially with the active  $d$  electrons of the bilayer.

### A. Bulk electronic structure

In the absence of SOC, a single crossing takes place along the  $\Gamma - M$  direction in both systems. Inspection of the band dispersion around those points reveals that the low-energy states form a Dirac cone. When SOC is introduced, a gap opens up at the crossing points (Fig. 1c,d), giving rise to a bulk insulating state.

The topological properties of the band structure can be characterized by calculating the topological invariant  $\nu$  associated with a system with time-reversal symmetry,

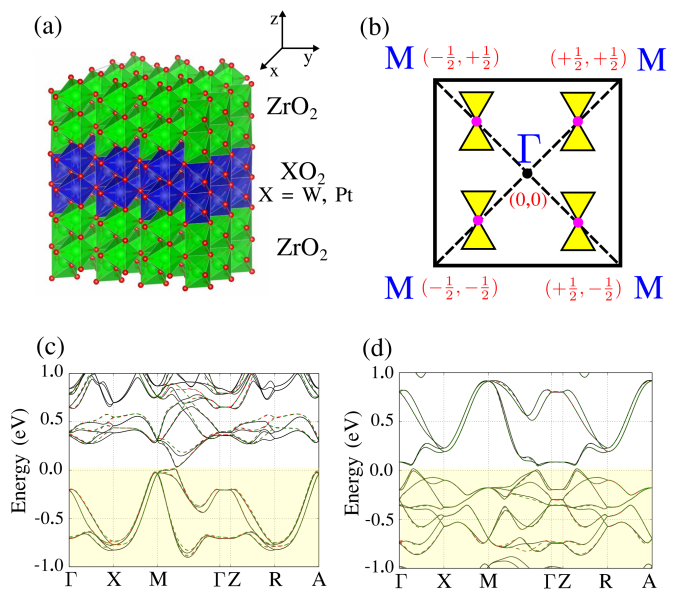


FIG. 1. (a) Sketch of the multilayer structure, based on the rutile unit cell, consisting of a bilayer of  $\text{WO}_2$  or  $\text{PtO}_2$  sandwiched between insulating  $\text{ZrO}_2$ . In the absence of spin-orbit coupling, the low-energy electronic properties are dominated by four Dirac equations located along the  $\Gamma - M$  path, as shown in the sketch (b). When SOC is introduced, the band structure develops a gap for both the W-based (c) and Pt-based (d) multilayers. The solid lines in (c,d) correspond to the DFT band structure, whereas the dashed lines correspond to the Wannier interpolation. In (d), the anti-crossing between  $\Gamma$  and X is already present without SOC.

by means of the  $Z_2$  invariant. In the case of crystals with inversion symmetry, it is known that the topological invariant can be obtained simply by calculating the parities of the wavefunctions at the time reversal invariant momenta (TRIM).<sup>23</sup> Nevertheless, the rutile structure presented here does not possess global inversion symmetry, but only in-plane, so that we cannot apply such procedure to the whole band structure. To calculate topological invariants for systems without inversion symmetry several methods have been proposed: (i) direct numerical calculation of the Pfaffian,<sup>24</sup> (ii) looking for an obstruction for a time-reversal smooth gauge<sup>25</sup> and (iii) Wannier charge center evolution.<sup>26,27</sup> We have chosen this latter method, since it is numerically highly stable and specially well suited for electronic structure calculations. It is based on following the flow of the Wannier charge centers as one moves across half of the Brillouin zone. With this scheme, an odd number of crossings of the Wannier charge centers label a non-trivial system, whereas an even number implies a trivial one.

From our calculations, we obtain that the charge centers cross an even number of times, implying that there is an even number of Kramers pairs per edge. Nevertheless, we observe that the charge centers can be separated in two families, each one showing an odd num-

ber of crossings, giving rise to a topological crystalline insulator.<sup>27,28</sup> Every family of Wannier centers, whose existence is related to the mirror symmetry of the unit cell, will produce a pair of Kramers edge states, adding up to a total of four edge states. The gapless nature of these edge states is not totally protected against perturbations even when they respect time-reversal symmetry, because perturbations mixing the two families, such as chemical edge reconstruction, will be able to open up an edge gap. This topological crystalline insulating phase is analogous to two coupled non-trivial quantum spin Hall states, as in bilayer graphene with spin-orbit coupling.<sup>29,30</sup> Importantly, topological insulating states, even if they are not protected against symmetry mixing perturbations, have been shown to be robust<sup>31–36</sup> against edge perturbations.

### B. Edge states

Having a bulk gapped spectrum and a crystalline topological invariant, the rutile structures are expected to show edge states when studied in a finite geometry. Using the Wannier Hamiltonian derived from the electronic structure calculations, we calculate the surface spectral function by solving Dyson's equation

$$G(k_x, E) = (E - H_0 - t^\dagger(k_x)G(k_x, E)t(k_x))^{-1} \quad (1)$$

where  $H_0$  is the matrix with the intra-cell matrix elements,  $k_x$  the vector parallel to the interface and  $t(k_x)$  the hopping of the Bloch Hamiltonian in the direction perpendicular to the interface. From the Green's function, the surface spectral function is calculated as  $\Gamma(k_x, E) = \frac{1}{\pi} \text{Im}(G(k_x, E))$ , and shown in Fig. 2 for the W- and Pt-based rutile multilayers.

The surface spectral function shows that both systems develop surface states, a total of four of them. The existence of four edge states is coherent with the interpretation that the electronic structure is equivalent to two coupled quantum spin Hall insulators. In a topological quantum spin Hall insulator, the number of surface states is 2 (or 6, 8...), so that the surface hosts a single Kramers pair, whose crossing cannot be avoided due to time-reversal symmetry. In our present case, due to the existence of two Kramers pairs, perturbations can gap out the surface states without breaking time-reversal symmetry. Kramers degeneracy holds at the TRIM ( $\Gamma$  and  $X$ ), where the two branches of edge states are degenerate in both valence and conduction band.

## III. TOPOLOGICAL INVARIANT IN RUTILES

While the opening of Dirac points is a well known route to engineer quantum spin Hall insulators, we have shown that in the present rutile multilayers quantum spin Hall states are realized that are not fully protected. In terms

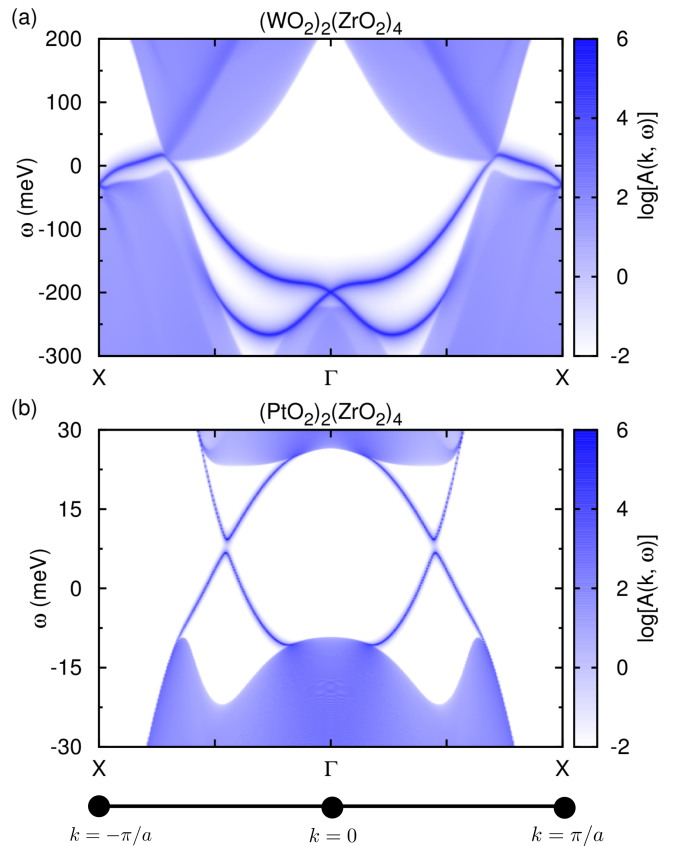


FIG. 2. Edge (01) k-resolved density of states for the W-based (a) and Pt-based multilayer (b). A set of edge states appear within the gap, but due to the lack of a strong topological index, their existence is not protected, developing a small gap.

of Wannier charge centers, the origin can be traced back to the additional symmetries of the system, namely mirror symmetry, that impose that there are two families of Wannier centers, each one yielding a pair of Kramers edge states. In terms of effective low energy Dirac points, the  $C_4$  symmetry imposes that the system has four spinless low energy Dirac points, yielding twice the number of conventional honeycomb lattices, and twice as many edge states. Therefore, the combination of time reversal,  $C_4$  and mirror symmetry, and low energy effective Dirac Hamiltonian, imposes that the system will show four edge states. In the following we will try to give an intuitive understanding of why this happens, as well as suggest a situation where a strong topological state can be obtained by modifying the symmetry of our material.

### A. Origin of the topological insulating state

Starting with the situation without spin-orbit coupling, the band structure is characterized by the four Dirac crossings introduced at the beginning. Independently of whether those crosses are Dirac, anisotropic

Dirac or semi-Dirac, the important feature for the present discussion is that they carry a  $\pm\pi$  Berry phase. We have verified numerically that for the non-SOC calculations, the Wannier Hamiltonians obtained generate Dirac-like crosses with  $\pm\pi$  Berry phase. The Dirac points are located along the  $\Gamma - M$  path (shown in Fig. 1b), where the position depends on the details of the electronic structure, giving rise to a total of four non-equivalent Dirac points in the full Brillouin zone.

In the presence of SOC, a spin-dependent mass term appears in the Hamiltonian. Due to the absence of inversion symmetry, the eigenvalues are not degenerate except at the TRIM points, where Kramers degeneracy is retained. This is reflected in the different masses for different Kramers states. It has been shown that the  $Z_2$  invariant can be related to the so-called spin Chern number, or simply to the Chern number  $C$  of one of the Kramers sectors. This can be easily understood in topological states where  $s_z$  is conserved, and the  $Z_2$  invariant is

$$\nu = C_{\uparrow} \pmod{2} \quad (2)$$

which in the case of monolayer graphene gives  $C_S = 2$ ,  $C_{\uparrow} = 1$  and  $\nu = 1$ , while for bilayer graphene it results in  $C_S = 4$ ,  $C_{\uparrow} = 2$  and  $\nu = 0$ . In the case of rutile multilayers, due to the existence of four gapped Dirac equations for each Kramers manifold, the Chern number for a certain Kramers manifold will be a sum over the Chern numbers of four Dirac equations  $C_i$ , which due to the  $\pm\pi$  Berry phase will be  $C_i = \pm 1/2$ . By labeling the Kramers manifold as  $\uparrow$  in analogy to the spin conserving case, we have

$$C_{\uparrow} = \sum_{i=1}^4 s_i \frac{1}{2} \quad (3)$$

where  $s_i = \pm 1$  depending on the sign of the SOC-induced Dirac masses. Due to the in-plane inversion symmetry, the Chern number of the different Dirac equations around  $+\vec{k}$  and  $-\vec{k}$  will be the same. We will have that  $C_1 = C_3 = s_1 \frac{1}{2}$  and  $C_2 = C_4 = s_2 \frac{1}{2}$ . Therefore, the Chern number for one of the Kramers sectors will be

$$C_{\uparrow} = s_1 + s_2 = 0, \pm 2 \quad (4)$$

With the previous Kramers Chern number, the topological invariant will result into  $\nu = 0$ , so that the system will not be a strong topological insulator in any case. For the case of  $C_{\uparrow} = +2$ , time reversal symmetry ( $C = 0$ ) imposes that the Chern number of the other sector is  $C_{\downarrow} = -2$ , giving a total  $C_S = 4$ , predicting four edge states. This last situation is precisely the one we obtained when calculating the edge spectra of the Pt- and W- multilayers.

We would like to emphasize that in the case of having a similar system but with magnetic order, so that a

single spin flavor is present at the Fermi level, the previous argument will predict that the total Chern number is 2. This has been explicitly calculated in a V-based magnetic rutile multilayer<sup>19</sup> that shows four semi-Dirac points along  $\Gamma - M$ , obtaining that the system is an anomalous Hall insulator showing two co-propagating edge states.<sup>19</sup> It is interesting to note that, contrary to other oxide systems,<sup>37</sup> in this system magnetism brings about the topological protection for the edge states, as time-reversal symmetry breaking leads to protected topological states.

The crystalline topological state in the time reversal Pt- and W- multilayers is therefore a consequence of the existence of a total of four Dirac points in the non-relativistic band structure. This compares with the case of honeycomb lattices, where usually only two Dirac equations are present, and the Chern number spin flavor is  $C_{\uparrow,\downarrow} = \pm 1$ . In these rutile-based nanostructures,  $C_4$  symmetry imposes that a total of 4 Dirac equations appear between  $\Gamma$  and  $M$ . If such symmetry is broken, it could be possible to have an electronic structure with only two Dirac equations that could give rise to a strong topological insulating phase. A way to realize that will be to expand the cell along the (11) direction. With such distortion, two of the Dirac points will displace differently than the other in k-space. In particular, they can open up a trivial gap, whereas the other two remain gapless (or with a much smaller gap). In that situation, switching on SOC might be able to create band inversion in two of the Dirac points, but not in the other two, giving rise to  $C_{\uparrow} = 1$  and robust quantum spin Hall state  $\nu = 1$ .

## B. Model Hamiltonian for spinless fermions

In the following we will illustrate the different topological states of the rutile lattice by means of a model Hamiltonian. We stress that the following model Hamiltonians do not intend to precisely capture the electronic structure of the two multilayers presented above, their goal is just to provide an intuitive understanding of the topology of the low-energy electronic structure. We choose a variation from a model previously shown to develop anisotropic Dirac points<sup>38</sup> in a similar system.

$$H_{\uparrow}(\vec{k}) = \begin{pmatrix} \epsilon_1(\vec{k}) & T(\vec{k}) \\ T^*(\vec{k}) & \epsilon_2(\vec{k}) \end{pmatrix} \quad (5)$$

with

$$\begin{aligned} \epsilon_1(k_x, k_y) &= -\epsilon + 2t(\cos k_x + \cos k_y) \\ \epsilon_2(k_x, k_y) &= \epsilon - 2t(\cos k_x + \cos k_y) \\ T(\vec{k}) &= V(\vec{k}) + W(\vec{k}) + Z(\vec{k}) \\ V(k_x, k_y) &= 2t'(\cos k_x - \cos k_y) \\ W(k_x, k_y) &= 2i\alpha \sin(k_x - k_y) \\ Z(k_x, k_y) &= 2i\lambda \sin k_x \sin k_y \end{aligned}$$

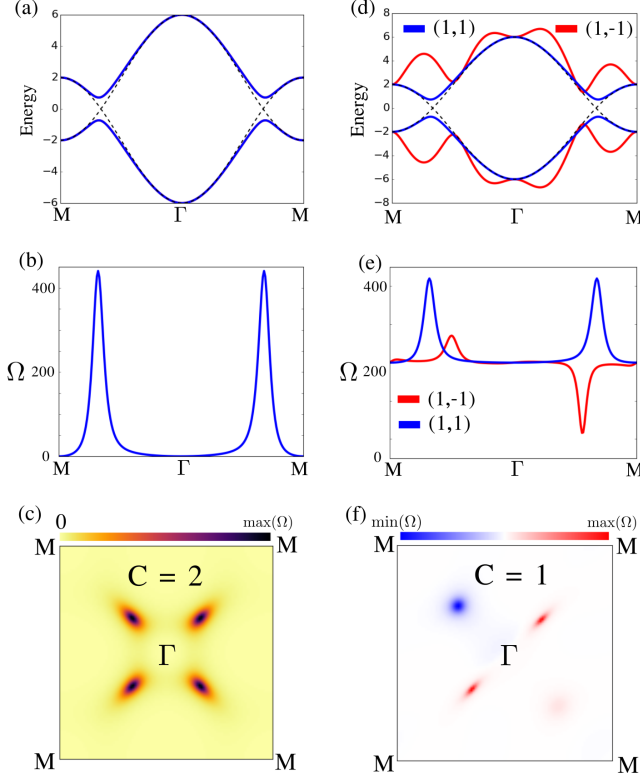


FIG. 3. Band structure (a) along the (1,1) direction for the model in Eq. 5, in the quantum anomalous ( $C = 2$ ) regime ( $\alpha = 0, \lambda \neq 0$ ), Berry curvature along the path (b) and in the whole Brillouin zone (c). Dashed lines in (a) show the bands for ( $\alpha = \lambda = 0$ ), the gapless regime. Band structure (d), and Berry curvatures (e,f) in the QAH regime with  $\alpha \neq 0, \lambda \neq 0$ , with total Chern number  $C = 1$ . Parameters are  $\epsilon = -2$ ,  $t = 1$ ,  $t' = 2, \lambda = 0.5$  and  $\alpha = 2$

The terms  $\epsilon_1, \epsilon_2, V$  correspond to a simplified version of anisotropic Dirac points.<sup>38</sup> The term  $W$  breaks the equivalence between the (1,1) and (1,-1) directions but conserves time reversal. The term  $Z$  breaks time-reversal symmetry, but maintains the equivalence between the (1,1) and (1,-1) directions. In the case of  $Z = W = 0$ , the previous Hamiltonian describes a band structure that shows four anisotropic Dirac points, located along the  $\Gamma - M$  directions. The Dirac nodes are equally spaced from  $\Gamma$  and occur at points  $\vec{k}_0 = (\kappa_1, \kappa_2)k_0$ , with  $\kappa_{1,2} = \pm 1$

We first focus on the case where  $W = 0$  ( $\alpha = 0$ ), but with a non-zero  $Z$  ( $\lambda \neq 0$ ) so that time-reversal symmetry is broken. In this situation, the band structure develops a gap (Fig. 3a), and the split Dirac points generate a non-zero Berry curvature (Fig. 3b). When integrated over the whole Brillouin zone, a Chern number  $C = 2$  is obtained. This situation is analogous to the one observed<sup>19</sup> in half-metallic V-based multilayers with SOC, a system that is also a QAH with  $C = 2$ , but with the difference that the low-energy electronic structure is of type *II* semi-Dirac<sup>19</sup>

instead of the anisotropic Dirac dispersion shown in Eq. 5.

If we first switch on the mirror-symmetry-breaking term  $W$ , the spectrum consists of two gapped Dirac equations in the (1,-1) direction with opposite Chern numbers, and two gapless Dirac equations in the (1,1) direction. If now time-reversal symmetry is broken by switching on  $Z$  ( $\lambda \neq 0$ ), and provided  $\lambda$  is not large enough to invert the gaps in (1,-1), the Dirac equation in the (1,1) will open up a gap with the same Chern number. The band structure for this situation is shown in Fig. 3d, where it is observed that the calculated Berry curvatures (Fig. 3e) and Chern number (Fig. 3f) are in agreement with the previous argument. Therefore, the model proposed in Eq. 5 shows a phase with Chern number  $C = 1$ , provided mirror symmetry is broken.

The previous phenomenology can be understood by expanding the Hamiltonian around the Dirac points.

$$H_\kappa = -\sigma_z p_1 + \kappa_1 \kappa_2 \sigma_x p_2 - \sigma_y m_\kappa \quad (6)$$

where  $m_\kappa$  is a mass term induced by  $W$  and  $Z$ ,  $p_1 = \kappa_1 p_x + \kappa_2 p_y$ ,  $p_2 = -\kappa_2 p_x + \kappa_1 p_y$ , with  $p_{x,y}$  the crystal momenta around the different valleys. The Chern number for the previous valley Hamiltonian can be written as

$$C_\kappa = \frac{1}{2} \text{sign}(\kappa_1 \kappa_2 m_\kappa) \quad (7)$$

In the case of  $\lambda \neq 0$  and  $\alpha = 0$ , we have  $m_\kappa = \kappa_1 \kappa_2 m$  so  $C_\kappa = 1/2$ , and when summing over the four valleys it gives  $C = 2$ . In the case of  $\alpha \neq 0$ , two of the valley Chern numbers can yield opposite signs, so that the net Chern number will be  $C = 1$ .

### C. Model Hamiltonian for quantum spin Hall

So far we have been studying a model for spinless fermions, showing that it leads to two different quantum anomalous Hall states. With the previous model a spinful time-reversal version can be built as

$$H(\vec{k}) = \begin{pmatrix} H_\uparrow(\vec{k}) & 0 \\ 0 & H_\downarrow(\vec{k}) \end{pmatrix} = \begin{pmatrix} H_\uparrow(\vec{k}) & 0 \\ 0 & H_\uparrow^*(-\vec{k}) \end{pmatrix} \quad (8)$$

With the previous ansatz the net Chern number is zero as imposed by time reversal, and the parameter  $\lambda$  can be now understood as arising from SOC. For  $\alpha = 0$ , following the discussion in Sec. III A, the spin Chern number yields  $C_S = 4$ , giving rise to a crystalline topological insulator (Fig. 4a), compatible with the DFT results presented in Fig. 1. Switching on the mirror symmetry term  $\alpha$ , the spin Chern number yields  $C_S = 2$ , giving rise to a strong topological insulator (Fig. 4b). Therefore, a



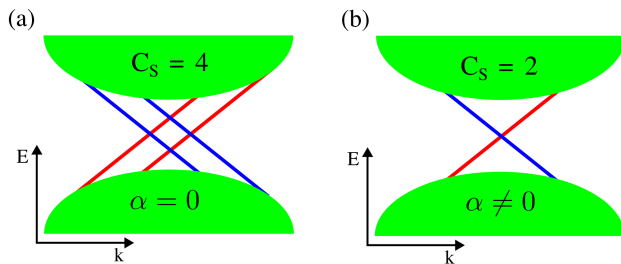


FIG. 4. Sketch of the edge states for the Hamiltonian Eq. 8, showing the crystalline insulating state with spin Chern number  $C_S = 4$  (a), and the strong phase with  $C_S = 2$ . The transition from (a) to (b) is driven by the mirror symmetry parameter  $\alpha$ . In a real material, such transition can be induced by strain in the (11) direction. The DFT results of Fig. 2 correspond to the symmetric case (a).

mirror-symmetry breaking term in our model Hamiltonian is capable of creating a quantum phase transition from the original crystalline topological insulating state to a strong topological insulator. We finally clarify that in the real materials introduced in this manuscript, spin mixing terms would show up in their effective Hamiltonian.

#### IV. CONCLUSIONS

We have shown that two rutile-based bilayers formed by an active 5d-electron system with  $5d^2$  and  $5d^6$  electron count host a crystalline topological insulating state. The origin of the non robust topological state comes from having four Dirac equations in the absence of SOC, in comparison with honeycomb lattices (whether this is graphene or oxide-based) that show only two. This limitation can be traced to the Chern number per Kramers sector, that in the rutile structure is 2 whereas in the honeycomb lattice is 1. We have suggested that by removing undesired Dirac points, it would be possible to design strong quantum spin Hall insulators in the rutile lattice. We have shown with a toy model calculation for spinless fermions that apart from the insulating phase

with  $C = 2$ , breaking in-plane mirror symmetry will allow to enter a state with  $C = 1$ . The extension of the previous model with mirror symmetry breaking to the spinful time-reversal case would give rise to a strong 2D topological insulator.

#### ACKNOWLEDGMENTS

J.L.L. acknowledges financial support from Marie-Curie-ITN 607904 SPINOGRAPH. D.G. and R.V. thank the Deutsche Forschungsgemeinschaft for funding through SFB/TR 49. V.P. thanks the Xunta de Galicia for financial support under the Emerxentes Program via Project No. EM2013/037 and the MINECO via Project No. MAT2013-44673-R. V.P. acknowledges support from the MINECO of Spain via the Ramon y Cajal program under Grant No. RyC-2011-09024. P.B. acknowledges partial support from the European Unions Horizon 2020 research and innovation programme under Grant Agreement No. 696656 GrapheneCore. We thank GEFES2016 for providing the platform for this collaboration to succeed.

#### Appendix A: Methods

We have carried out density functional theory (DFT) calculations with various codes: WIEN2k,<sup>39</sup> and Quantum Espresso<sup>40</sup> for the various cell and geometry relaxations plus the electronic structure analysis (both codes yielding comparable results), and using the code FPLO<sup>41</sup> for relativistic Wannierization calculations. Structural relaxations using both WIEN2k and Quantum Espresso were carried out with the PBE version of the generalized gradient approximation<sup>42</sup> as an exchange-correlation functional, using PAW pseudopotentials in the QE case and a full-potential calculation with WIEN2k, both without SOC. The construction of Wannier functions was performed within the full-relativistic version of FPLO using a  $6 \times 6 \times 3$   $k$ -point grid. For the  $(\text{WO}_2)_2/(\text{ZrO}_2)_n$  case we included all Zr 4d and W 5d states. For the  $(\text{PtO}_2)_2/(\text{ZrO}_2)_n$  case we included all Zr 4d, O 2p and Pt 5d states.

\* jose.luis.lado@gmail.com

† guterding@itp.uni-frankfurt.de

<sup>1</sup> M. Z. Hasan and C. L. Kane, “Colloquium : Topological insulators,” *Rev. Mod. Phys.*, vol. 82, pp. 3045–3067, Nov 2010.

<sup>2</sup> X.-L. Qi and S.-C. Zhang, “Topological insulators and superconductors,” *Rev. Mod. Phys.*, vol. 83, pp. 1057–1110, Oct 2011.

<sup>3</sup> C. L. Kane and E. J. Mele, “Quantum spin hall effect in graphene,” *Phys. Rev. Lett.*, vol. 95, p. 226801, Nov 2005.

<sup>4</sup> L. Fu and C. L. Kane, “Superconducting proximity effect and majorana fermions at the surface of a topological insulator,” *Phys. Rev. Lett.*, vol. 100, p. 096407, Mar 2008.

<sup>5</sup> S. R. Elliott and M. Franz, “Colloquium : Majorana fermions in nuclear, particle, and solid-state physics,” *Rev. Mod. Phys.*, vol. 87, pp. 137–163, Feb 2015.

<sup>6</sup> Z. Wang, H. Zhang, D. Liu, C. Liu, C. Tang, C. Song, Y. Zhong, J. Peng, F. Li, C. Nie, *et al.*, “Topological edge states in a high-temperature superconductor fese/srtio3 (001) film,” *Nature Materials*, 2016.

- <sup>7</sup> J. Sinova, S. O. Valenzuela, J. Wunderlich, C. H. Back, and T. Jungwirth, “Spin hall effects,” *Rev. Mod. Phys.*, vol. 87, pp. 1213–1260, Oct 2015.
- <sup>8</sup> B. A. Bernevig, T. L. Hughes, and S.-C. Zhang, “Quantum spin hall effect and topological phase transition in hgte quantum wells,” *Science*, vol. 314, no. 5806, pp. 1757–1761, 2006.
- <sup>9</sup> M. König, S. Wiedmann, C. Brüne, A. Roth, H. Buhmann, L. W. Molenkamp, X.-L. Qi, and S.-C. Zhang, “Quantum spin hall insulator state in hgte quantum wells,” *Science*, vol. 318, no. 5851, pp. 766–770, 2007.
- <sup>10</sup> H. Zhang, C.-X. Liu, X.-L. Qi, X. Dai, Z. Fang, and S.-C. Zhang, “Topological insulators in bi<sub>2</sub>se<sub>3</sub>, bi<sub>2</sub>te<sub>3</sub> and sb<sub>2</sub>te<sub>3</sub> with a single dirac cone on the surface,” *Nature physics*, vol. 5, no. 6, pp. 438–442, 2009.
- <sup>11</sup> B.-J. Yang and Y. B. Kim, “Topological insulators and metal-insulator transition in the pyrochlore iridates,” *Phys. Rev. B*, vol. 82, p. 085111, Aug 2010.
- <sup>12</sup> Z. Wang, N. Su, and F. Liu, “Prediction of a two-dimensional organic topological insulator,” *Nano letters*, vol. 13, no. 6, pp. 2842–2845, 2013.
- <sup>13</sup> L. Wei, X. Zhang, and M. Zhao, “Spin-polarized dirac cones and topological nontriviality in a metal-organic framework ni<sub>2</sub>c<sub>24</sub>s<sub>6</sub>h<sub>12</sub>,” *Physical Chemistry Chemical Physics*, vol. 18, no. 11, pp. 8059–8064, 2016.
- <sup>14</sup> X. Li, E. Zhao, and W. V. Liu, “Topological states in a ladder-like optical lattice containing ultracold atoms in higher orbital bands,” *Nature communications*, vol. 4, p. 1523, 2013.
- <sup>15</sup> D. Xiao, W. Zhu, Y. Ran, N. Nagaosa, and S. Okamoto, “Interface engineering of quantum hall effects in digital transition metal oxide heterostructures,” *Nature communications*, vol. 2, p. 596, 2011.
- <sup>16</sup> J. L. Lado, V. Pardo, and D. Baldomir, “*Ab initio* study of Z<sub>2</sub> topological phases in perovskite (111) (sr<sub>2</sub>io<sub>3</sub>)<sub>7</sub>/(sriro<sub>3</sub>)<sub>2</sub> and (ktao<sub>3</sub>)<sub>7</sub>/(kpto<sub>3</sub>)<sub>2</sub> multilayers,” *Phys. Rev. B*, vol. 88, p. 155119, Oct 2013.
- <sup>17</sup> Q.-F. Liang, L.-H. Wu, and X. Hu, “Electrically tunable topological state in [111] perovskite materials with an antiferromagnetic exchange field,” *New Journal of Physics*, vol. 15, no. 6, p. 063031, 2013.
- <sup>18</sup> H.-M. Guo and M. Franz, “Three-dimensional topological insulators on the pyrochlore lattice,” *Phys. Rev. Lett.*, vol. 103, p. 206805, Nov 2009.
- <sup>19</sup> H. Huang, Z. Liu, H. Zhang, W. Duan, and D. Vanderbilt, “Emergence of a chern-insulating state from a semi-dirac dispersion,” *Phys. Rev. B*, vol. 92, p. 161115, Oct 2015.
- <sup>20</sup> J. F. Afonso and V. Pardo, “*Ab initio* study of nontrivial topological phases in corundum-structured (M<sub>2</sub>O<sub>3</sub>)/(Al<sub>2</sub>O<sub>3</sub>)<sub>5</sub> multilayers,” *Phys. Rev. B*, vol. 92, p. 235102, Dec 2015.
- <sup>21</sup> D. Guterding, H. O. Jeschke, and R. Valentí, “Prospect of quantum anomalous hall and quantum spin hall effect in doped kagome lattice mott insulators,” *Scientific reports*, vol. 6, p. 25988, 2016.
- <sup>22</sup> V. Pardo and W. E. Pickett, “Half-metallic semi-dirac-point generated by quantum confinement in tio<sub>2</sub>/vo<sub>2</sub> nanostructures,” *Phys. Rev. Lett.*, vol. 102, p. 166803, Apr 2009.
- <sup>23</sup> L. Fu and C. L. Kane, “Topological insulators with inversion symmetry,” *Phys. Rev. B*, vol. 76, p. 045302, Jul 2007.
- <sup>24</sup> M. Wimmer, “Algorithm 923: efficient numerical computation of the pfaffian for dense and banded skew-symmetric matrices,” *ACM Transactions on Mathematical Software (TOMS)*, vol. 38, no. 4, p. 30, 2012.
- <sup>25</sup> T. Fukui and Y. Hatsugai, “Quantum spin hall effect in three dimensional materials: Lattice computation of z<sub>2</sub> topological invariants and its application to bi and sb,” *Journal of the Physical Society of Japan*, vol. 76, no. 5, p. 053702, 2007.
- <sup>26</sup> A. A. Soluyanov and D. Vanderbilt, “Computing topological invariants without inversion symmetry,” *Phys. Rev. B*, vol. 83, p. 235401, Jun 2011.
- <sup>27</sup> D. Gresch, G. Autes, O. V. Yazyev, M. Troyer, D. Vanderbilt, B. A. Bernevig, and A. A. Soluyanov, “Z2pack: Numerical implementation of hybrid wannier centers for identifying topological materials,” *arXiv preprint arXiv:1610.08983*, 2016.
- <sup>28</sup> L. Fu, “Topological crystalline insulators,” *Phys. Rev. Lett.*, vol. 106, p. 106802, Mar 2011.
- <sup>29</sup> E. Prada, P. San-Jose, L. Brey, and H. Fertig, “Band topology and the quantum spin hall effect in bilayer graphene,” *Solid State Communications*, vol. 151, no. 16, pp. 1075–1083, 2011.
- <sup>30</sup> N. A. García-Martínez, J. L. Lado, and J. Fernández-Rossier, “Quantum spin hall phase in multilayer graphene,” *Phys. Rev. B*, vol. 91, p. 235451, Jun 2015.
- <sup>31</sup> D. Xiao, W. Yao, and Q. Niu, “Valley-contrasting physics in graphene: Magnetic moment and topological transport,” *Phys. Rev. Lett.*, vol. 99, p. 236809, Dec 2007.
- <sup>32</sup> M. Sui, G. Chen, L. Ma, W.-Y. Shan, D. Tian, K. Watanabe, T. Taniguchi, X. Jin, W. Yao, D. Xiao, *et al.*, “Gate-tunable topological valley transport in bilayer graphene,” *Nature Physics*, vol. 11, no. 12, pp. 1027–1031, 2015.
- <sup>33</sup> Z. Qiao, J. Jung, Q. Niu, and A. H. MacDonald, “Electronic highways in bilayer graphene,” *Nano letters*, vol. 11, no. 8, pp. 3453–3459, 2011.
- <sup>34</sup> J. Li, K. Wang, K. J. McFaul, Z. Zern, Y. Ren, K. Watanabe, T. Taniguchi, Z. Qiao, and J. Zhu, “Gate-controlled topological conducting channels in bilayer graphene,” *Nature Nanotechnology*, 2016.
- <sup>35</sup> J. Li, I. Martin, M. Büttiker, and A. F. Morpurgo, “Topological origin of subgap conductance in insulating bilayer graphene,” *Nature Physics*, vol. 7, no. 1, pp. 38–42, 2011.
- <sup>36</sup> Z. Ringel, Y. E. Kraus, and A. Stern, “Strong side of weak topological insulators,” *Phys. Rev. B*, vol. 86, p. 045102, Jul 2012.
- <sup>37</sup> S. Okamoto, W. Zhu, Y. Nomura, R. Arita, D. Xiao, and N. Nagaosa, “Correlation effects in (111) bilayers of perovskite transition-metal oxides,” *Phys. Rev. B*, vol. 89, p. 195121, May 2014.
- <sup>38</sup> S. Banerjee, R. R. P. Singh, V. Pardo, and W. E. Pickett, “Tight-binding modeling and low-energy behavior of the semi-dirac point,” *Phys. Rev. Lett.*, vol. 103, p. 016402, Jul 2009.
- <sup>39</sup> K. Schwarz, P. Blaha, and G. Madsen, “Electronic structure calculations of solids using the wien2k package for material sciences,” *Computer Physics Communications*, vol. 147, no. 1, pp. 71–76, 2002.
- <sup>40</sup> P. Giannozzi, S. Baroni, N. Bonini, M. Calandra, R. Car, C. Cavazzoni, D. Ceresoli, G. L. Chiarotti, M. Cococcioni, I. Dabo, *et al.*, “Quantum espresso: a modular and open-source software project for quantum simulations of materials,” *Journal of physics: Condensed matter*, vol. 21, no. 39, p. 395502, 2009.
- <sup>41</sup> K. Koepnik and H. Eschrig, “Full-potential nonorthogonal local-orbital minimum-basis band-structure scheme,” *Phys. Rev. B*, vol. 59, pp. 1743–1757, Jan 1999.

- <sup>42</sup> J. P. Perdew, K. Burke, and M. Ernzerhof, “Generalized gradient approximation made simple,” *Phys. Rev. Lett.*, vol. 77, pp. 3865–3868, Oct 1996.